University for their advice and support. We thank Max Brandt for linguistic revision. This study received financial support from Akademiska Sjukhuset, Uppsala University, Uppsala, Sweden.

REFERENCES

1. Boring CC, Squires TS, Tong T, Montgomery S. Cancer statistics. *CA Cancer J Clin* 1994;44:7-26.
2. Jaklitsch M, Strauss G, Healey E, DeCamp M, Liptay M, Sugarbaker D. An historical perspective of multi-modality treatment for resectable non-small cell lung cancer. *Lung Cancer* 1995;12:S17-S32.
3. Non-small CLCG. Chemotherapy in non-small cell lung cancer: a meta-analysis using updated data on individual patients from 52 randomized clinical trials. *BMJ* 1995;311: 899-909.
4. Williams A, Santiago S, Lehrman S, Popper R. Transcutaneous needle aspiration of solitary pulmonary masses: how many passes? *Am Rev Respir Dis* 1987;136:452-454.
5. Winning A, McIvor J, Seed WA, Husain O, Metaxas N. Interpretation of negative results in fine needle aspiration of discrete pulmonary lesions. *Thorax* 1986;41:875-879.
6. Wang K, Kelly S, Britt J. Percutaneous needle aspiration biopsy of chest lesions. New instrument and new technique. *Chest* 1988;93:993-997.
7. Schenk D, Bryan C, Bower J, Myers D. Transbronchial needle aspiration in the diagnosis of bronchogenic carcinoma. *Chest* 1987;92:83-85.
8. Polak J, Kubik A. Percutaneous thin needle biopsy of malignant and non-malignant thoracic lesions. *Radiologia Diagnostica* 1989;30:177-182.
9. Webb WR. Radiologic evaluation of the solitary pulmonary nodule. *Am J Roentgenol* 1990;154:701-708.
10. Scott WJ, Gobar LS, Hauser LG, Sunderland JJ, Dewan NA, Sugimoto JT. Detection of scalene lymph node metastases from lung cancer. Positron emission tomography. *Chest* 1995;107:1174-1176.
11. Webb WR, Gatsonis C, Zerhouni EA, et al. CT and MR imaging in staging non-small cell bronchogenic carcinoma: report of the Radiologic Diagnostic Oncology Group. *Radiology* 1991;178:705-713.
12. Swensen SJ, Morin RL, Schueler BA, et al. Solitary pulmonary nodule: CT evaluation of enhancement with iodinated contrast material—a preliminary report. *Radiology* 1992;182:343-347.
13. Bragg DG. Current applications of imaging procedures in the patient with lung cancer. *Int J Radiat Oncol Biol Phys* 1991;21:847-851.
14. Strauss LG, Conti PS. The applications of PET in clinical oncology. *J Nucl Med* 1991;32:623-648.
15. Wahl RL, Hutchins GD, Buchsbaum DJ, Liebert M, Grossman HB, Fisher S. Fluorine-18-2-deoxy-2-fluoro-D-glucose uptake into human tumor xenografts. Feasibility studies for cancer imaging with positron emission tomography. *Cancer* 1991; 67:1544-1550.
16. Nolop K, Rhodes C, Brudin L, et al. Glucose utilization in vivo by human pulmonary neoplasm. *Cancer* 1987;60:2682-2689.
17. Scott WJ, Schwabe JL, Gupta NC, Dewan NA, Reeb SD, Sugimoto JT. Positron emission tomography of lung tumors and mediastinal lymph nodes using [^{18}F]fluorodeoxyglucose. The members of the PET lung tumor study group. *Ann Thorac Surg* 1994;58:698-703.
18. Abe Y, Matsuzawa T, Fujiwara T, et al. Clinical assessment of therapeutic effects on cancer using ^{18}F-2-fluoro-2-deoxy-D-glucose and positron and emission tomography: preliminary study of lung cancer. *Int J Radiat Oncol Biol Phys* 1990;19:1005-1010.
19. Slosman DO, Spiliopoulos A, Couson F, et al. Satellite PET and lung cancer: a prospective study in surgical patients. *Nucl Med Commun* 1993;14:955-961.
20. Patz EF Jr, Lowe VJ, Hoffman JM, et al. Focal pulmonary abnormalities: evaluation with ^{18}F-fluorodeoxyglucose PET scanning. *Radiology* 1993;188:487-490.
21. Dewan NA, Gupta NC, Redepenning LS, Phalen JJ, Frick MP. Diagnostic efficacy of PET-F-FDG imaging in solitary pulmonary nodules. Potential role in evaluation and management. *Chest* 1993;104:997-1002.
22. Fujiwara T, Matsuzawa T, Kubota K, et al. Relationship between histologic type of primary lung cancer and carbon-11-L-methionine uptake with positron emission tomography. *J Nucl Med* 1989;30:33-37.
23. Kubota K, Matsuzawa T, Ito M, et al. Lung tumor imaging by positron emission tomography using ^{11}C-L-methionine. *J Nucl Med* 1985;26:37-42.
24. Kubota K, Matsuzawa T, Fujiwara T, et al. Differential diagnosis of lung tumor with positron emission tomography: a prospective study. *J Nucl Med* 1990;31:1927-1932.
25. Kubota K, Yamada S, Ishiwata K, Ito M, Ido T. Positron emission tomography for treatment evaluation and recurrence detection compared with CT in long-term follow-up cases of lung cancer. *Clin Nucl Med* 1992;17:877-881.
26. Rhodes CG, Wollmer P, Fazio F, Jones TJ. Quantitative measurement of regional extravascular lung density using positron emission and transmission tomography. *J Comput Assist Tomogr* 1981;5:783-791.
27. Långström B, Antoni G, Gullberg P, et al. Synthesis of l- and d-[Isqb]methyl-^{11}C]methionine. *J Nucl Med* 1987;28:1037-1040.
28. Mulholland G, Toorongian S, Jewett D, Bachelor M, Kilbourn M. Routine production of 2-deoxy-2[Isqb]^{18}F]Fluoro-d-glucose by direct nucleophilic exchange on a quaternary 4-aminopyridinum resin. *Nucl Med Biol* 1990;17:273.
29. Kops E, Herzog H, Schmid A, Holte S, Feinendegen L. Performance characteristics of an eight-ring whole body PET scanner. *J Comput Assist Tomogr* 1990;14:437-445.
30. Patlak C, Blasberg R, Fenstermacher J. Graphic evaluation of blood-to-brain transfer constants from multiple-time uptake data. *J Cerebr Blood Flow Metab* 1983;3:1-7.
31. Hatazawa J, Ishiwata K, Itoh M, et al. Quantitative evaluation of L-[Isqb]methyl-^{11}C-]-methionine uptake in tumor using positron emission tomography. *J Nucl Med* 1989;30:1809-1813.
32. Hübner KF, Buonocore E, Singh SK, Gould HR, Cotten DW. Characterization of chest masses by F-FDG positron emission tomography. *Clin Nucl Med* 1995;20:293-298.
33. Rege SD, Hoh CK, Glaspy JA, et al. Imaging of pulmonary mass lesions with whole-body positron emission tomography and fluorodeoxyglucose. *Cancer* 1993;72: 82-90.
34. Dewan NA, Reeb SD, Gupta NC, Gobar LS, Scott WJ. PET-F-FDG imaging and transthoracic needle lung aspiration biopsy in evaluation of pulmonary lesions. A comparative risk-benefit analysis. *Chest* 1995;108:441-446.
35. Patz EF Jr, Lowe VJ, Hoffman JM, Paine SS, Harris LK, Goodman PC. Persistent or recurrent bronchogenic carcinoma: detection with PET and 2-[Isqb]F-18]-2-deoxy-D-glucose. *Radiology* 1994;191:379-382.
36. McLoud TC, Bourgouin PM, Greenberg RW, et al. Bronchogenic carcinoma: analysis of staging in the mediastinum with CT by corrective lymph node mapping and sampling. *Radiology* 1991;182:319-323.
37. Wahl RL, Quint LE, Greenough RL, Meyer CR, White RI, Orringer MB. Staging of mediastinal non-small cell lung cancer with F-FDG PET, CT, and fusion images: preliminary prospective evaluation. *Radiology* 1994;191:371-377.

Iodine-131-Metaiodobenzylguanidine Uptake in Metastatic Carcinoid Tumor to the Orbit

Michael W. Hanson, Andrew M. Schneider, David S. Enterline, Jerome M. Feldman and Jon P. Gockerman

Division of Nuclear Medicine, Department of Radiology, Divisions of Endocrinology and Oncology, Department of Medicine, Duke University Medical Center, Durham, North Carolina

Metastatic tumor is one of several etiologies of space-occupying masses in the orbit that accounts for 1%–13% of all orbital masses (*1*). In the adult patient population, breast cancer is the most common tumor to metastasize to the orbit followed by metastases from the lung, prostate and gastrointestinal tract (*2*). It is rare for carcinoid tumors to metastasize to the eye or to the orbit. Carcinoid tumors arise from Kulchitsky cells that originate in the neural crest. Histologically, these tumors resemble, but are not as aggressive as, adenocarcinomas. Most carcinoids arise in the gastrointestinal tract or the lung. The most common site for carcinoid metastases is the liver. On anatomical imaging studies, such as CT and magnetic resonance imaging, metastatic orbital carcinoid tumors appear as nonspecific tumor masses. Carcinoid tumors have an affinity for uptake of the radiopharmaceutical ^{131}I-metaiodobenzylguanidine (MIBG) (*3*). We report a case of a patient with a known carcinoid tumor who developed a left orbital mass that demonstrated abnormal uptake of ^{131}I-MIBG indicative of metastatic carcinoid tumor to the orbit.

Key Words: carcinoid tumor; orbital metastasis; iodine-131 metaiodobenzylguanidine

J Nucl Med 1998; 39:647–650

Received Dec. 16, 1996; revision accepted Apr. 14, 1997.

For correspondence or reprints contact: Michael W. Hanson, MD, Department of Radiology, Division of Nuclear Medicine, P.O. Box 3949, Duke University Medical Center, Durham, NC 27710.

CASE REPORT

A 76-yr-old man presented with a history of peripheral visual impairment of his left eye for 2 yr and diplopia for 3 mo. Twenty-three years prior to presentation, the patient had a carcinoid tumor diagnosed following a resection of a mesenteric mass found incidentally at the time of an appendectomy for acute appendicitis. Follow-up surgery, after resection of the small mesenteric mass, revealed a 3.2-cm primary carcinoid tumor of the ileum that was resected along with part of the ileum and colon. Retroperitoneal lymph nodes were positive for a carcinoid tumor. Subsequent laboratory analysis revealed elevated urinary excretion of 5-hydroxyindoleacetic acid (5-HIAA) and elevated platelet serotonin concentration.

Clinically, the patient had tolerated his carcinoid for many years and had only required therapy for symptom relief primarily related to diarrhea. He had not required antineoplastic chemotherapy. Other medical problems included recurrent gastrointestinal bleeding from varices at the junction of his ileal anastomosis, a myocardial infarction, hyperthyroidism and pulmonary tuberculosis. At the time of imaging, physical examination revealed proptosis and strabismus of his left eye and an inability to adduct his left eye. A brain magnetic resonance imaging (MRI) study revealed a left orbital mass.

Subsequently, a whole-body ^{131}I-metaiodobenzylguanidine (MIBG) scan and a dedicated orbital MRI scan were obtained. The MRI scan (Signa 1.5 T, 5.4 software; General Electric, Milwaukee, WI) (Fig. 1) demonstrated a 2.0 × 2.7 × 1.8-cm mass lesion in the medial left orbit that involved both the medial rectus and superior oblique muscles. There was left orbital proptosis. The left globe and the optic nerve were laterally displaced though not infiltrated. Intraconal fat signal was normal. The right orbit was normal. Images from the whole-body ^{131}I-MIBG scan acquired on a 180° opposing dual-head gamma camera (Vision T-22: SMV America; Twinsburg, OH) at 24 and 48 hr after the intravenous injection of 74.0 MBq (2.0 mCi) of ^{131}I-MIBG are shown in Figures 2 and 3. These images demonstrated multiple areas of abnormal ^{131}I-MIBG accumulation that included the peritoneum, liver, pericardium and left superior mediastinum/supraclavicular region. Asymmetric tracer accumulation in the region of the parotid glands was due to prior surgical removal of the right parotid gland. There was prominent focal abnormal accumulation of ^{131}I-MIBG in the medial left orbit corresponding to the mass in this location on the MRI.

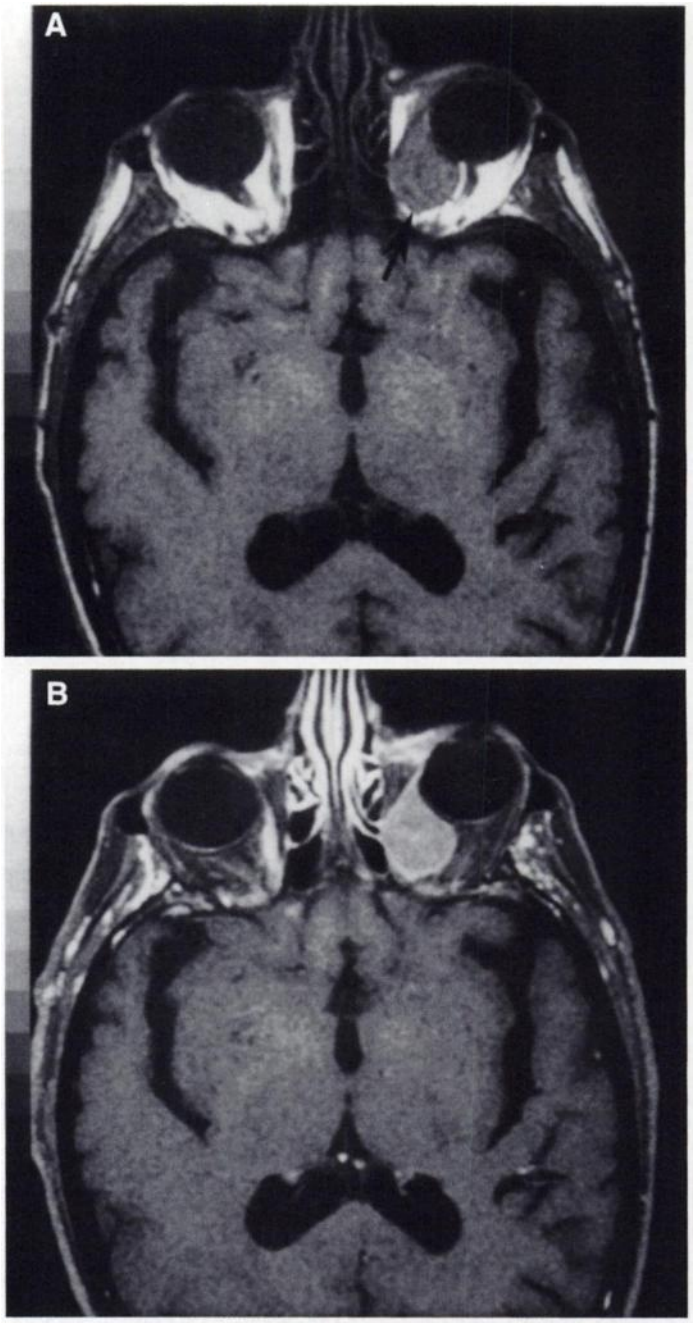

FIGURE 1. (A) Axial T1-weighted MRI of the orbit. There is an expansile left orbital mass involving the medial rectus muscle (arrow), which is isointense to the extraoccular muscles. (B) Axial T1-weighted fat-suppressed MRI of the orbit. The left orbital mass homogeneously enhances.

DISCUSSION

The MRI is the anatomical imaging modality of choice for orbital imaging. Its main advantage is its ability to provide exquisite soft tissue contrast that generates differential characteristics of orbital tumors that cannot be distinguished by CT. Other advantages include the multiplanar imaging capability of MRI, the lack of ionizing radiation and the avoidance of iodinated contrast agents (*4*).

Despite the ability of MRI to differentiate many different tumors by MR signal characteristics, a definitive tumor diagnosis is often not possible with MRI alone. MRI of orbital metastatic lesions, in general, usually demonstrates an irregular, infiltrating and nonencapsulated tumor that often involves the extraocular muscles. However, metastatic carcinoid may demonstrate a well-circumscribed appearance (*5*). Metastatic tumors typically have an isointense T1 signal and a mildly hyperintense T2 signal relative to the extraocular muscles (*5*). Orbital carcinoid metastases, however, can show decreased signal intensity on T2-weighted images (*5*). Other tumors with similar signal characteristics to the carcinoid include idiopathic inflammatory orbital pseudotumor, Graves' ophthalmopathy and rhabdomyosarcoma (*6*). There are no specific MRI signal characteristics that distinguish the orbital metastatic carcinoid tumor.

Carcinoid tumors belong to a group of tumors known as Apudomas, all of which are thought to arise from cells in the neural crest. This group of tumors share many characteristics including the presence of a cell membrane neuronal pump mechanism that allows the cells to accumulate norepinephrine. Norepinephrine is stored in neurosecretory granules and is subsequently secreted. Some of the secreted norepinephrine is taken up by adrenergic cells and stored again in these granules. The success of ^{131}I-MIBG as an imaging agent is derived from its chemical similarities to norepinephrine, with which it com-

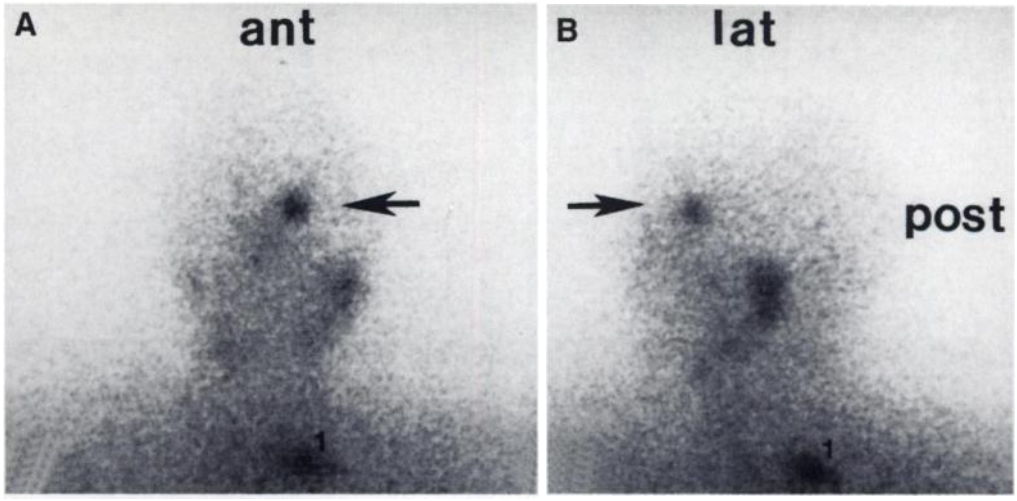

FIGURE 2. (A) Anterior and (B) left lateral ^{131}I-MIBG images of the head and neck. There is prominent focal abnormal ^{131}I-MIBG accumulation in the medial left orbit (arrows) and the left supraclavicular region (*1*).

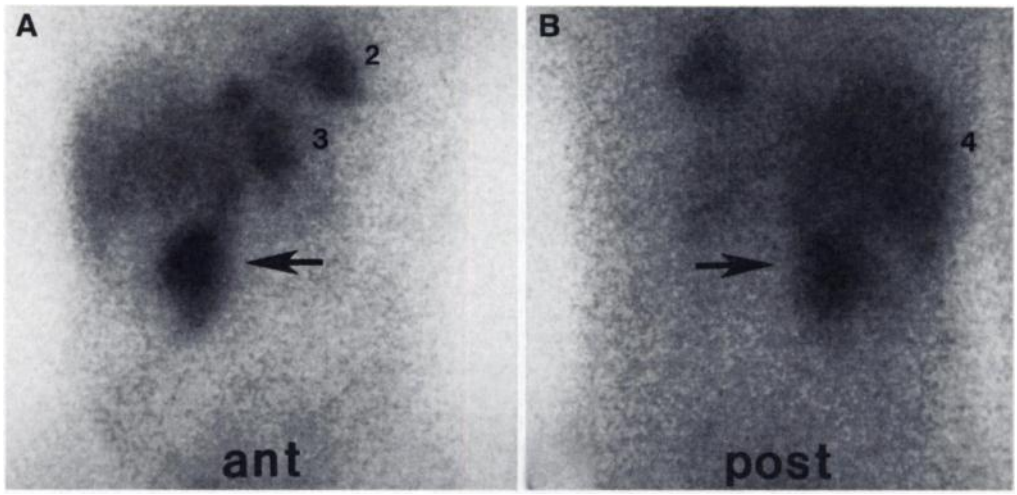

FIGURE 3. (A) Anterior and (B) posterior ^{131}I-MIBG images of the abdomen. There are scattered foci of abnormal ^{131}I-MIBG accumulation in pericardium, (2) left lobe of liver, (3) right lobe of liver (4) and prominent focal area of abnormal ^{131}I-MIBG accumulation in right peritoneum (arrows).

petes, as they both enter the metabolic pathway into and out of the adrenergic tissues. Though not specific solely for carcinoids, the abnormal accumulation of ^{131}I-MIBG has a high specificity for this group of tumors.

The first successful imaging of carcinoid tumors with ^{131}I-MIBG was performed by Fisher et al. (*3*) in 1984. Since then, several investigators have reported successful imaging of carcinoid tumors with ^{131}I-MIBG (*7–10*). Previous studies from our laboratory have shown that 59% of all patients with carcinoid tumors had abnormal ^{131}I-MIBG scans. In a subset of our patients with carcinoid tumors who had an elevation of their serum serotonin level, as many as 80% had abnormal ^{131}I-MIBG scans (*8*). Mandigers et al. (*11*) have reported the case of a patient with a tumor arising in the middle ear, which, by biopsy, was initially classified by the referring hospital as a paraganglioma. Urinary 5-HIAA was markedly elevated, and an ^{123}I-MIBG scan showed prominent focal increased tracer accumulation at the location of the tumor. A repeat biopsy was performed. Immunohistochemistry revealed a clear positive reaction with antibodies directed against several markers including serotonin. A revised diagnosis of a carcinoid tumor was made. Mandigers et al. (*11*) recommended urinary screening for catecholamines and 5-HIAA in all patients with paragangliomas of the head and neck and, if elevated levels are found, the patient should undergo whole-body imaging with MIBG.

CONCLUSION

Although rare in its occurrence, metastatic carcinoid to the orbit must be a diagnostic consideration in patients who present with an orbital mass and known metastatic carcinoid tumor. Other pathology must also be considered that cannot be excluded adequately by the findings on CT or MRI alone. Additional information that could further characterize these orbital masses would be helpful to evaluate these patients. The additional information that can be gained from the whole-body ^{131}I-MIBG scan includes: (a) additional specificity and increased confidence in a noninvasive diagnosis of metastatic carcinoid as the etiology of the mass identified on CT or MRI, (b) identification and localization of other sites of metastatic carcinoid detected by the whole-body imaging capabilities of ^{131}I-MIBG and (c) determination of the ^{131}I-MIBG uptake characteristics of the orbital mass in consideration for possible administration of high-dose ^{131}I-MIBG therapy (*12,13*).

REFERENCES

1. Shields JA. *Diagnosis and management of orbital tumors*. Philadelphia: W.B. Saunders Co., 1989:291.
2. Shields CL, Shields JA, Peggs M. Metastatic tumors to the orbit. *Ophthal Reconstr Plast Surg* 1988;4:73–80.
3. Fischer M, Kamanabroo D, Sonderkamp H, Proske T. Scintigraphic imaging of carcinoid tumours with ^{131}I-metaiodobenzylguanidine [Letter]. *Lancet* 1984;2:165.
4. DePotter P, Flanders AE, Shields CL, Shields JA. Magnetic resonance imaging of orbital tumors. *Int Ophthal Clinics* 1993;33:163–173.
5. DePotter P, Shields JA, Shields CL. *MRI of the eye and orbit*. Philadelphia: J.B. Lippincott Company, 1995:237–238.
6. Braffman BH, Bilaniuk LT, Eagle RC Jr, et al. MR imaging of a carcinoid tumor metastatic to the orbit. *J Comput Assist Tomogr* 1987;11:891–894.
7. Hoefnagel CA, Jager DH, Van Gennip AH, Marcuse HR, Taal BG. Diagnosis and treatment of a carcinoid tumor using iodine-131 metaiodobenzylguanidine. *Clin Nucl Med* 1986;11:150–152.
8. Hanson MW, Feldman JM, Blinder RA, Moore JO, Coleman RE. Carcinoid tumors: iodine-131 MIBG scintigraphy. *Radiology* 1989;172:699–703.

9. Watanabe N, Seto H, Ishiki M, et al. Iodine-123 MIBG imaging of metastatic carcinoid tumor from the rectum. *Clin Nucl Med* 1995;20:357–360.
10. Hirano T, Otake H, Watanabe N, et al. Presurgical diagnosis of a primary carcinoid tumor of the thymus with MIBG. *J Nucl Med* 1995;36:2243–2245.
11. Mandigers CMPW, van Gils APG, van der Mey AGL, Hogendoorn PCW. Carcinoid tumor of the jugulo-tympanic region. *J Nucl Med* 1996;37:270–272.
12. Hoefnagel CA, Taal BG, Valdes Olmos RA. Role of ^{131}I-metaiodobenzylguanidine therapy in carcinoids. *J Nucl Biol Med* 1991;35:346–348.
13. Taal BG, Hoefnagel CA, Valdes Olmos RA, Boot H, Beijnen JH. Palliative effect of metaiodobenzylguanidine in metastatic carcinoid tumors. *J Clin Oncol* 1996;14:1829–1838.

Prostate Cancer Abdominal Metastases Detected with Indium-111 Capromab Pendetide

George H. Hinkle, John K. Burgers, John O. Olsen, Bonnie S. Williams, Renita A. Lamatrice, Rolf F. Barth, Barbara Rogers and Robert T. Maguire

Departments of Radiology and Pathology, The Ohio State University Medical Center, Columbus; Urologic Surgeons, Inc., Columbus, Ohio; and Cytogen Corporation, Princeton, New Jersey

To provide appropriate therapy for prostate cancer, accurate staging of the patient's disease is essential. Determination of tumor size, location, periprostatic extension and metastatic disease in the skeleton and soft tissue are needed to stage properly. Current diagnostic modalities may lead to understaging in 40%–70% of prostate cancer. Detection of metastatic disease, both at the time of initial diagnosis and in patients with suspected local recurrence, can significantly alter the type of therapy given. Clinical studies using the ^{111}In radiolabeled immunoconjugate, MAb 7E11-C5.3-GYK-DTPA (capromab pendetide), have shown the superiority of radioimmunoscintigraphy over other diagnostic modalities in the detection of both primary and metastatic prostate cancer. Radioimmunoscintigraphy with capromab pendetide depends on expression of tumor-associated antigen rather than lesion size. Earlier detection of extraprostatic invasion and metastases by means of radioimmunoscintigraphy provides valuable information for treatment decisions. A case of metastatic prostate cancer in the abdomen of a patient without local disease, in which the extent of disease was confirmed at autopsy after sudden cardiac arrest, is presented.

Key Words: prostate cancer; indium-111; capromab pendetide; radioimmunoscintigraphy

J Nucl Med 1998; 39:650-652

CASE REPORT

A 50-yr-old man was found on routine physical examination to have an elevated prostate-specific antigen (PSA) level (20.3 ng/ml) and an enlarged prostate by digital rectal examination. After biopsy, the initial diagnosis was moderately-to-poorly differentiated prostatic carcinoma involving both lobes. His past medical history was otherwise unremarkable and he was not taking any medication. CT of the abdomen and pelvis and a radionuclide bone scan revealed no evidence of metastatic disease. A radical prostatectomy was performed, and histopathologic examination showed a solitary micrometastasis in a left obturator lymph node. Moderately differentiated (Gleason 6) adenocarcinoma was found in both prostatic lobes. Local margins were free of tumor including urethral and bladder margins (Stage 4, T3, N1, M0). Postoperatively, the patient did well clinically and his postoperative 1-mo PSA level was < 0.5 ng/ml. However, 5 mo after surgery, the PSA had increased to 1.4 ng/ml and at 8 mo it had risen to 2.4 ng/ml. Needle biopsy of the prostatic bed was negative. Radionuclide bone scan disclosed no evidence of skeletal metastatic disease.

The patient was enrolled in a clinical study involving radioimmunoscintigraphy with ^{111}In capromab pendetide. This recently FDA-approved radiopharmaceutical is composed of the antibody, 7E11.C5, which recognizes PSMA or prostate-specific membrane antigen (*1*). At this time, his PSA level was 6.1 ng/ml and peroxidase-antiperoxidase (PAP) level was 0.3 U/liter. No other lab values were abnormal. The patient denied bone pain, weight loss and urologic symptoms. An MRI of the abdomen and pelvis showed no evidence of lymphadenopathy. The patient received 203.5 MBq (5.5 mCi) ^{111}In capromab pendetide and whole-body and SPECT images were completed 4 days later. Uptake was noted in the upper abdomen at the level of the upper pole of the left kidney (Figs. 1 and 2). A second finding was an increased uptake at the aortic bifurcation (Figs. 2 and 3).

Based on these results, the patient was started on hormonal therapy. Four days later, he died at home of sudden cardiac arrest. At autopsy, no grossly residual tumor was identified in the pelvic cavity. Several enlarged periaortic lymph nodes were found in the upper left abdomen corresponding to positive uptake on the nuclear medicine images. Metastatic prostate cancer was identified in two of these, as well as in two of four nodes at the level of the aortic bifurcation. A solitary 1-cm nodule with central necrosis that was shown to be a benign adenoma was identified in the lower pole of the left kidney.

Samples of the tumor-positive periaortic and aortic-bifurcation lymph nodes were sent for PSMA and PSA expression determination along with a portion of the left kidney mass. Two lymph nodes from the aortic bifurcation area showed approximately 70% of the cells positive for PSMA with moderate (2+) to strong (3+) staining intensity. All tumor cells also were PSA (+) and displayed strong (3+) stain intensity. A third lymph node from the same area was negative for both tumor and PSMA and PSA staining. Two lymph nodes from the periaortic area showed 90% of the tumor cells positive for PSMA with moderate (2+) to strong (3+) staining intensity. A small foci of tumor in a third lymph node also stained positive for PSMA. All three nodes stained 100% for PSA with a strong (3+) staining intensity. As expected, the adenoma of the left kidney was nonreactive.

Received Mar. 11, 1997; revision accepted May 8, 1997.
For correspondence or reprints contact: George H. Hinkle, MS, RPh, Department of Radiology, The Ohio State University Medical Center, Rm. 203D, Doan Hall, 410 West Tenth Ave., Columbus, OH 43210.